Bioorganic & Medicinal Chemistry Letters 19 (2009) 251–254

Contents lists available at ScienceDirect

Bioorganic & Medicinal Chemistry Letters

journal homepage: www.elsevier.com/locate/bmcl

Molecular modeling of the α9α10 nicotinic acetylcholine receptor subtype

Edwin G. Pérez [a,c], Bruce K. Cassels [a,c], Gerald Zapata-Torres [b,c,*]

[a] Department of Chemistry, Faculty of Sciences, University of Chile, Casilla 653, Santiago, Chile
[b] Department of Inorganic and Analytical Chemistry, Faculty of Chemical and Pharmaceutical Sciences, University of Chile, Olivos 1007, Independencia, Santiago, Chile
[c] Millennium Institute for Cell Dynamics and Biotechnology, Beauchef 861, Santiago, Chile

ARTICLE INFO

Article history:
Received 6 August 2008
Accepted 20 October 2008
Available online 25 October 2008

Keywords:
Nicotinic acetylcholine receptors
Nicotine
Acetylcholine
α-Conotoxin RgIA
Molecular dynamics

ABSTRACT

This study reports the comparative molecular modeling, docking and dynamic simulations of human α9α10 nicotinic acetylcholine receptors complexed with acetylcholine, nicotine and α-conotoxin RgIA, using as templates the crystal structures of Aplysia californica and Lymnaea stagnalis acetylcholine binding proteins. The molecular dynamics simulations showed that Arg112 in the complementary α10(−) subunit, is a determinant for recognition in the site that binds small ligands. However, Glu195 in the principal α9(+), and Asp114 in the complementary α10(−) subunit, might confer the potency and selectivity to α-conotoxin RgIA when interacting with Arg7 and Arg9 of this ligand.

The nicotinic acetylcholine receptors (nAChRs) are ligand-gated ion channels found throughout the body, where they mediate fast synaptic transmission. The nAChRs are responsible for mediating the effects of the neurotransmitter acetylcholine (ACh) and are also the principal target of nicotine (Nic), which typically, though not always, mimics the effects of ACh on them. Classically, nAChRs have been divided into two groups: muscle and neuronal receptors. The former are found at the skeletal neuromuscular junction, where they mediate neuromuscular transmission, and the latter are present throughout the central and peripheral nervous system.[1] The nAChRs are pentameric proteins comprising either combinations of two different types of subunits (α and β) or five copies of the same α subunit symmetrically arranged around a central ion pore. So far, nine different types of α subunit (α2–α10) and three kinds of β subunits (β2–β4) have been cloned and characterized as constituents of neuronal nAChRs.[2]

The nAChRs play crucial physiologic roles throughout the central and peripheral nervous system. They regulate neurotransmitter release, cell excitability, neuronal integration and networking, and are intimately involved in such important functions as sleep and arousal patterns, fatigue, hunger, anxiety, and pain processing.[1,3–5] Dysfunction of nAChRs is implicated in a variety of human disease conditions, including epilepsy, tobacco addiction, schizophrenia, myasthenia gravis, and some forms of skin disorders.[3,6] Their function most likely extends beyond the boundaries of neural function since they have also been identified in such diverse tissues as lymphocytes and keratinocytes.[6,7]

The inner ear hair cell α9α10 nAChR is a unique receptor because it is formed by two different α subunits. It has a characteristic mixed nicotinic-muscarinic pharmacologic profile and is sensitive to a broad range of ligands.[8,9] Studies on the α9α10 nAChR have greatly enhanced our understanding of nAChR function, the efferent olivocochlear pathway, and auditory hair cell function and development.[10,11] Recently, it has been reported that the inner ear requires α9α10 nAChRs to permit CNS modulation of cochlear mechanics.[12] Further, the nAChR α9α10 clearly has a function outside of the auditory system, though this precise function remains to be fully elucidated. Recent studies have defined the importance of these receptors in physiology, indicating that they represent an important component of human diseases and are thus potential targets for the therapy of a variety of ear disorders, including the prevention, and/or treatment of noise-induced hearing loss, as well as debilitating disorders as vertigo or tinnitus.[13]

In this paper we describe the comparative homology models, docking and molecular dynamics simulations (MD) of the ligand-binding domain (LBD) of α9α10 nAChR with ACh, Nic and α-conotoxin RgIA (RgIA) to shed light on possible ligand–receptor interactions.

Sequence alignments. For the small ligands ACh and Nic, a sequence alignment was generated between the sequences extracted from the X-ray crystal structure of nicotine-bound to *Lymnaea stagnalis* acetylcholine binding protein (*Ls*-AChBP, PDB entry 1UW6) at 2.20 Å resolution[14] and the amino terminal domains of human α3, α9, α10, α7, β2, and β4 nAChRs by means of the CLUSTALW package applying default parameters.[16] For conotoxin α-RgIA, using the same procedure, a second sequence alignment

* Corresponding author. Tel.: +56 2 9782961; fax: +56 2 7370567.
E-mail address: gzapata@uchile.cl (G. Zapata-Torres).

0960-894X/$ - see front matter © 2008 Elsevier Ltd. All rights reserved.
doi:10.1016/j.bmcl.2008.10.094

was generated between the sequences extracted from the X-ray crystal structure of *Aplysia californica* acetylcholine binding protein (*Ac*-AChBP-IMI, PDB entry 2C9T) at 2.25 Å resolution.[15] Although the sequence identity between the AChBP and the human nAChR LBD is relatively low (18–26%), the presence of highly conserved ACh binding residues in the AChBP[17] and the reported nicotinic pharmacology for *Ls*-AChBP[18] suggest that our comparative homology modeling of the nAChR LBD using the AChBP structure is appropriate.

With the sequence alignments at hand and the retrieved crystal structures of 1UW6 and 2C9T X-ray as templates, the program MODELLER (version 9v3)[19] was used to build the 3D models of the LBD of human α9α10 nAChR according to the comparative protein modeling method. In order to retain the complementarities between subunits at their interfaces, all five subunits were modeled simultaneously with the reported stoichiometry $(\alpha9)_2(\alpha10)_3$.[20] Thus, the formed pentamer, with the sequence α9α10α9α10α10, holds five probable ligand-binding sites in the interfaces corresponding to two α9(+)α10(−), two α10(+)α9(−) and one α10(+)α10(−) subunit pairs. In the obtained models, and using Autodock4.0 (AD4),[21] Nic and ACh were placed in a single binding site (α9(+)α10(−) interface) while keeping all other possible binding sites empty. It is worth noting that preliminary attempts to dock the RgIA peptide at the five binding site interfaces did not display its predicted potency, selectivity,[22] or the reported interactions for similar peptides according to the published X-ray structures.[15,23] Therefore, using MODELLER, we built the combined model nAChR α9α10-RgIA, using the *Ac*-AChBP-α conotoxin IMI structure as a template.

Molecular dynamics simulations. In order to determine the accuracy of our α9α10 nAChR LBD model, we performed MD simulations as follows: the LBD structure was solvated in an octahedral box of TIP3P water molecules,[24] with a minimum solute-wall distance of 10 Å. Different numbers of counterions were combined with the different net charges to produce neutral systems that closely resemble the physiological conditions of 0.10 M Na^+ and 0.05 M Cl^- ions. The total number of atoms of the MD-simulated system was 57,014 (including 3578 water molecules) for the solvated LBD of the α9α10 nAChR-small ligand complexes and 63,915 (including 5486 water molecules) for the solvated LBD of the α9α10 nAChR-RgIA complex. The MD simulations were performed using the Sander module of Amber9,[25] according to procedures already used for modeling other protein–ligand systems.[26] After six equilibration stages, each MD production was kept running for 5 ns with periodic boundary conditions in the *NTP* ensemble at $T = 300$ K with Berendsen temperature coupling and at $P = 1$ atm with isotropic molecule-based scaling.[27]

Structural models for α9α10 nAChR. The sequence alignments (see Fig. 1) revealed that most of the amino acid residues belonging to the binding sites in the AChBPs (*Ls* and *Ac*) and all nAChRs subunits used in our alignment are well conserved in type and position. The positions of the residues forming the typical aromatic cage,[14] at the bottom of the binding pocket, including Tyr88, Trp144, Tyr185, Tyr192, and the disulfide at positions 187 and 188 of the C loop of the principal (+) binding side, are well conserved. Moreover, Trp50 of the complementary (−) binding side that forms part of the aromatic cage is also well conserved. However, a major structural difference between α9α10 and other nAChRs occurs precisely in the complementary (−) binding side at the 112-position. In Figure 1 it can be seen that this position is occupied by a polar and large amino acid residue (Arg112) in α10 but a short and hydrophilic amino acid residue (Thr112) in α9. This position corresponds to Gln117 in α7 (a hydrophilic amino acid residue), Phe117 in β2 (an aromatic residue) and Leu117 in β4 (a hydrophobic one). The non-classical pharmacological behavior of Nic at the α9α10 nAChR could be explained by this striking difference. Examination of residues near to the complementary (−) binding site revealed another significant difference at position 114, the presence of a negatively charged Asp residue. This residue is present only in the α9 and α10 subunits and it has been predicted to play a critical role in the interaction of RgIA with α9α10 nAChR with regard to its high selectivity for this subtype.[28]

The best homology model obtained for the α9α10 nAChR was used for docking studies of small ligands by means of the AD4 program using default parameters described elsewhere.[21] Arg112 in the complementary subunit α10(−) was selected as the fully flexible residue, since according to experimental evidence residues in this location influence the interaction displayed by the ligands upon binding.[26] Once the best final docked energies were obtained for Nic and ACh, the complexed structures were further subjected to MD simulations with only one ligand in the α9(+)α10(−) interface. As the complex between α9α10 nAChR-RgIA using AD4 did not succeed, then the best scored α9α10 nAChR-RgIA model obtained by MODELLER was used for the MD process instead.

The MD simulation runs for both α9α10-ACh and α9α10-Nic complexes were very different. This result is not at all surprising since these ligands have dissimilar pharmacological profiles upon receptor binding, where ACh is an α9α10 agonist whilst Nic acts as an antagonist.[8,11] In addition, ACh displayed the same well-established cation-π interaction with the Trp143 residue;[14,29] however, Nic is completely removed from the agonist binding site (see Fig. 2A and B).

Also from the MD runs, it can be noted that the microscopic binding structure for α9α10 nAChR-ACh shows that the aromatic cage residues were maintained in similar positions but the mentioned Arg112 in the complementary α10(−) binding site forms a long hydrogen bond (2.92 Å) with the ACh carbonyl oxygen. The distance between the aromatic ring of Trp143 and the ammonium nitrogen moiety forming the cation-π interaction is ca. 4.80 Å, as reported in the literature.[14,29] Other interesting features of this

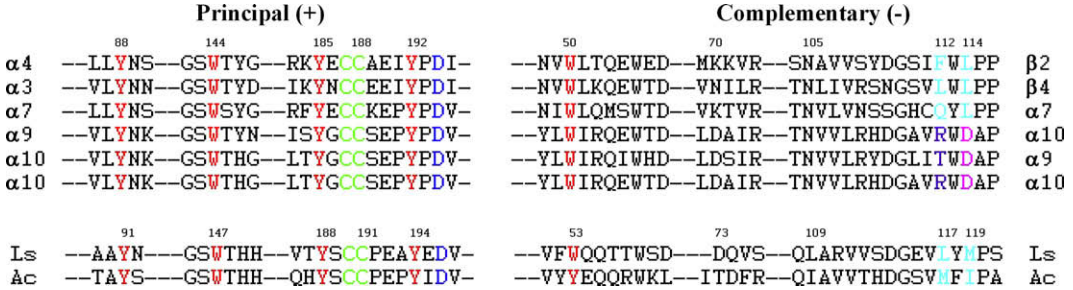

Figure 1. Sequence alignment of the amino acid residues around binding sites for the subunits of α9α10 and other nAChR subtypes with the reported ACh binding protein from *Aplysia californica* (Ac) and *Lymnaea stagnalis* (*Ls*). Aromatic nest residues colored red. Cystine bridge colored green. Residues in the binding site that are different in various subtypes are colored cyan, magenta and pink.

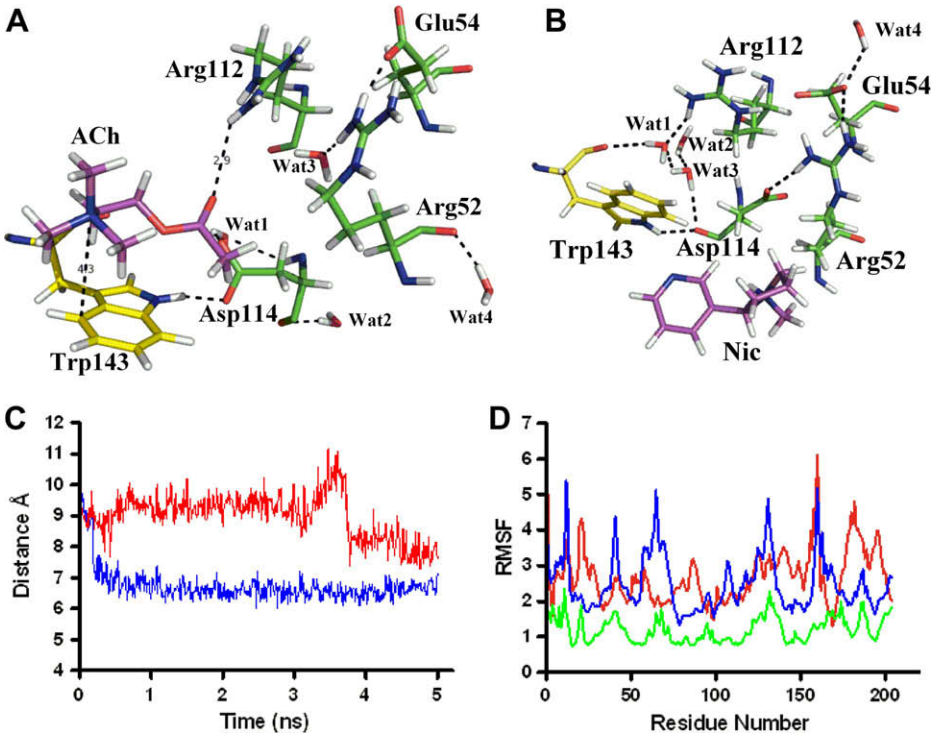

Figure 2. (A) Microscopic binding of the α9α10-ACh complex after MD. (B) Microscopic binding of the α9α10-Nic complex after MD. (C) NE(Arg112)-O(Trp143) distance: ACh (red) and Nic (blue). (D) RMSF (for the α9 subunit) showing the regions with major movements: ACh (red), Nic (blue) and RgIA (green).

system are two pairs of water molecules present in the binding site, where they form a pattern of hydrogen bonds with the polar side chains of Asp114 and Arg54 in the complementary α10(−) binding site.

On the contrary, the microscopic binding structure for α9α10 nAChR-Nic showed that, as a consequence of the side chain movement of Trp143 in the α9(+) subunit towards the aromatic cage, thus diminishing the crevice's volume, Nic moves away from its initial position. This movement allows for the formation of a hydrogen bond between the carbonyl oxygen of α9(+) Trp143 with a water molecule, which in turn forms another hydrogen bond with Arg112 of subunit α10(−). This water-mediated hydrogen bond pattern between these two residues keeps them both in a very stable conformation. This can be seen for one of their NE(Arg112) in the α10(−) subunit and the (Trp143) carbonyl oxygen in the α9(+) subunit. It is evident from Figure 2C that in the α9α10-ACh complex Arg112 remains ca. 9 Å from Trp143 and it takes nearly 5 ns to form the direct interaction. On the other hand, in the α9α10-Nic complex, this distance falls to ca. 6.5 Å after only about 0.25 ns. It is worth noting that this region must be constituted by highly polar residues, as can be inferred by the three water molecules present in this site.

The behaviors for Nic and RgIA are very similar, but different RMSF values are found, as shown in Figure 2D. In both cases the larger fluctuations are in surface regions identified as α-helix 1, the Cys loop and loop F, explaining the antagonist behavior of Nic at these receptors. The smaller RMSF values observed for RgIA indicate a greater number of interactions, as expected for a peptide bound to the surface of α9α10 nAChRs. ACh, on the contrary, destabilizes β-sheets 9 and 10, which are connected through loop C, in agreement with the activity of the endogenous agonist.[30]

When it comes to describing the microscopic binding structure for α9α10 nAChR-RgIA, a different set of interactions must be described compared with ACh and Nic since the peptide establishes interactions with both subunits. Although subtle amino acid differences can be observed with the IMI structure and certainly most of the interactions can be reproduced as described by the crystal structures, one mutation in RgIA with regard to IMI can explain the high selectivity shown by this peptide. In the 2BYP crystal, another IMI-*Ac* structure,[23] the guanidinium group of Arg7 establishes two salt bridges: an internal one with Asp5 and the other with Asp198; however in crystal structure 2C9T not only is the internal salt bridge seen, but in addition a hydrogen bond is observed with the carbonyl group of Ile194. In our MD run simulations, Arg7 of RgIA forms three interactions summarizing both crystal structures described above. The first one corresponds to the intra-residue salt bridge formed with Asp5, which should render a stable conformation for RgIA, a second salt bridge with α9(+) Asp198 (Asp195 in *Ac*-AChBP), and a third one corresponding to a hydrogen bond with the carbonyl group of Pro197 in the α9(+)

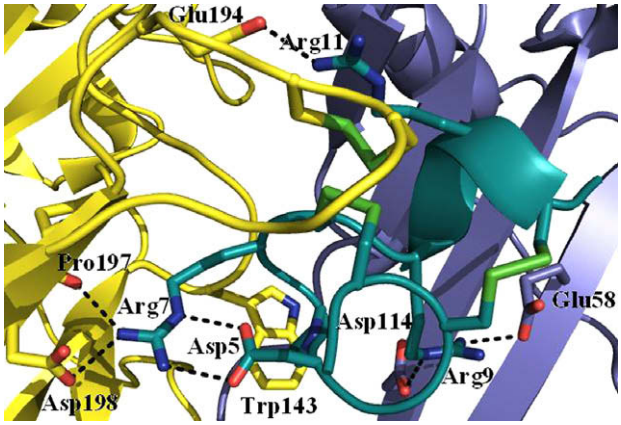

Figure 3. Main interactions of α-conotoxin RgIA (colored green) with principal α9(+) (colored yellow) and complementary α10(−) (colored blue) subunits after 5 ns of MD simulations.

subunit (Ile194 in *Ac*-AChBP). In a recent paper by Ellison et al., it has been demonstrated that the triad Asp5, Pro6, and Arg7 located in loop 1 of the peptide, are critical residues for the blockade of the both α9α10 and α7 subtypes.[31] A similar interaction has been described by Dutertre et al. for AChBP-α-TxIA (Arg5 in TxIA).[32] Also, Ellison et al. showed that Arg9 in loop 2 is critical for specific binding to the α9α10 subtype. In our MD simulations this residue forms two salt bridges with Glu58 and Asp114 in the α10(−) subunit. It worth noting that the latter residue is only present in the α9 and α10 subtypes, a circumstance which could argue in favor of the high selectivity shown by RgIA and also be an indication of how good an approximation MD is to describe the α9α10 system (see Fig. 3).

Acknowledgments

This work was funded by DI Grant 2006 INI 06/03-2 and ICM Grant No. P99-031-F. E.G.P. is grateful for a DAAD scholarship and GZ-T acknowledges a CONICYT (Chile) 'Proyecto Bicentenario de Inserción Académica' (2004).

References and notes

1. Gotti, C.; Clementi, F. *Prog. Neurobiol.* **2004**, *74*, 363.
2. Romanelli, M. N.; Gratteri, P.; Guandalini, L.; Martini, E.; Bonaccini, C.; Gualtieri, F. *ChemMedChem* **2007**, *2*, 746.
3. Lindstrom, J. *Mol. Neurobiol.* **1997**, *15*, 193.
4. Changeux, J. P.; Edelstein, S. J. *Curr. Opin. Neurobiol.* **2001**, *11*, 521.
5. Hogg, R. C.; Raggenbass, M.; Bertrand, D. *Rev. Physiol. Biochem. Pharmacol.* **2003**, *147*, 1.
6. Nguyen, V. T.; Ndoye, A.; Grando, S. A. *Am. J. Pathol.* **2000**, *157*, 1377.
7. Peng, H. S.; Ferris, R. L.; Matthews, T.; Hiel, H.; Lopez-Albaitero, A.; Lustig, L. R. *Life Sci.* **2004**, *76*, 263.
8. Elgoyhen, A. B.; Vetter, D. E.; Katz, E.; Rothlin, C. V.; Heinemann, S. F.; Boulter, J. *Proc. Natl. Acad. Sci. U.S.A.* **2001**, *98*, 3501.
9. Rothlin, C. V.; Lioudyno, M. I.; Silbering, A. F.; Plazas, P. V.; Casati, M.; Katz, E.; Guth, P. S.; Elgoyhen, A. B. *Mol. Pharmacol.* **2003**, *63*, 1067.
10. Baker, E. R.; Zwart, R.; Sher, E.; Millar, N. S. *Mol. Pharmacol.* **2004**, *65*, 453.
11. Gomez-Casati, M. E.; Fuchs, P. A.; Elgoyhen, A. B.; Katz, E. *J. Physiol. Lond.* **2005**, *566*, 103.
12. Vetter, D. E.; Katz, E.; Maison, S. F.; Taranda, J.; Turcan, S.; Ballestero, J.; Liberman, M. C.; Elgoyhen, B.; Boulter, J. *Proc. Natl. Acad. Sci. U.S.A.* **2007**, *104*, 20594.
13. Lustig, L. R. *Anat. Rec. Part A-Discov. Mol. Cell. Evol. Biol.* **2006**, *288A*, 424.
14. Celie, P. H. N.; van Rossum-Fikkert, S. E.; van Dijk, W. J.; Brejc, K.; Smit, A. B.; Sixma, T. K. *Neuron* **2004**, *41*, 907.
15. Ulens, C.; Hogg, R. C.; Celie, P. H.; Bertrand, D.; Tsetlin, V.; Smit, A. B.; Sixma, T. K. *Proc. Natl. Acad. Sci. U.S.A.* **2006**, *103*, 3615.
16. Thompson, J. D.; Gibson, T. J.; Plewniak, F.; Jeanmougin, F.; Higgins, D. G. *Nucl. Acids Res.* **1997**, *25*, 4876.
17. Brejc, K.; van Dijk, W. J.; Klaassen, R. V.; Schuurmans, M.; van der Oost, J.; Smit, A. B.; Sixma, T. K. *Nature* **2001**, *411*, 269.
18. Smit, A. B.; Syed, N. I.; Schaap, D.; van Minnen, J.; Klumperman, J.; Kits, K. S.; Lodder, H.; van der Schors, R. C.; van Elk, R.; Sorgedrager, B.; Brejc, K.; Sixma, T. K.; Geraerts, W. P. M. *Nature* **2001**, *411*, 261.
19. Sali, A.; Blundell, T. L. *J. Mol. Biol.* **1993**, *234*, 779.
20. Plazas, P. V.; Katz, E.; Gomez-Casati, M. E.; Bouzat, C.; Elgoyhen, A. B. *J. Neurosci.* **2005**, *25*, 10905.
21. Huey, R.; Morris, G. M.; Olson, A. J.; Goodsell, D. S. *J. Comp. Chem.* **2007**, *28*, 1145.
22. Ellison, M.; Olivera, B. M. *Chem. Rec.* **2007**, *7*, 341.
23. Hansen, S. B.; Sulzenbacher, G.; Huxford, T.; Marchot, P.; Taylor, P.; Bourne, Y. *EMBO J.* **2005**, *24*, 3635.
24. Jorgensen, W. L.; Chandrasekhar, J.; Madura, J. D.; Impey, R. W.; Klein, M. L. *J. Chem. Phys.* **1983**, *79*, 926.
25. Ponder, J. W.; Case, D. A. *Prot. Simulations* **2003**, *66*.
26. Huang, X. Q.; Zheng, F.; Chen, X.; Crooks, P. A.; Dwoskin, L. P.; Zhan, C. G. *J. Med. Chem.* **2006**, *49*, 7661.
27. Berendsen, H. J. C.; Postma, J. P. M.; Vangunsteren, W. F.; Dinola, A.; Haak, J. R. *J. Chem. Phys.* **1984**, *81*, 3684.
28. Olivera, B. M. *J. Biol. Chem.* **2006**, *281*, 31173.
29. Cashin, A. L.; Petersson, E. J.; Lester, H. A.; Dougherty, D. A. *J. Am. Chem. Soc.* **2005**, *127*, 350.
30. Liu, X.; Xu, Y.; Li, H.; Wang, X.; Jiang, H.; Barrantes, F. J. *PLoS Comp. Biol.* **2008**, *4*, 100.
31. Ellison, M.; Feng, Z. P.; Park, A. J.; Zhang, X.; Olivera, B. M.; McIntosh, J. M.; Norton, R. S. *J. Mol. Biol.* **2008**, *377*, 1216.
32. Dutertre, S.; Ulens, C.; Buttner, R.; Fish, A.; van Elk, R.; Kendel, Y.; Hopping, G.; Alewood, P. F.; Schroeder, C.; Nicke, A.; Smit, A. B.; Sixma, T. K.; Lewis, R. J. *EMBO J.* **2007**, *26*, 3858.